In-situ measurement of electron energy evolution in a laser-plasma accelerator

S. Bohlen,[1,2,*] T. Brümmer,[1] F. Grüner,[2] C. A. Lindstrøm,[1] M. Meisel,[1,2] T. Staufer,[2] M.J.V. Streeter,[1,3] M. Veale,[4] J.C. Wood,[1] R. D'Arcy,[1] K. Põder,[1] and J. Osterhoff[1]

[1] *Deutsches Elektronen-Synchrotron DESY, Notkestr. 85, 22607 Hamburg, Germany*
[2] *Universität Hamburg, Luruper Chaussee 149, 22761 Hamburg, Germany*
[3] *Centre for Plasma Physics, School of Mathematics and Physics, Queen's University Belfast, BT7 1NN, Belfast United Kingdom*
[4] *STFC, Rutherford Appleton Laboratory, Harwell Science & Innovation Campus, Didcot, OX11 0QX*

(Dated: August 20, 2021)

We report on a novel, non-invasive method applying Thomson scattering to measure the evolution of the electron beam energy inside a laser-plasma accelerator with high spatial resolution. The determination of the local electron energy without altering the final beam state enabled the in-situ detection of the acting acceleration fields, in this Letter demonstrated in a plasma density ramp varying from $(265 \pm 119)\,\mathrm{GV/m}$ to $(9 \pm 4)\,\mathrm{GV/m}$. The presented data shows excellent agreement with particle-in-cell simulations. This method provides new possibilities for detecting dynamics of plasma-based accelerators and their optimization.

In laser-plasma acceleration (LPA) [1] electric fields on the order of 100 GV/m can be generated for the acceleration of electron bunches to highly relativistic energies over short distances. As such, plasma-based accelerators outperform the acceleration gradients achieved in radio-frequency (RF) devices by orders of magnitude. After the first demonstration of quasi mono-energetic beams in 2004 [2–4], the energy frontier of LPA has been pushed continuously [5–7], now reaching more than 8 GeV [8], within range of state-of-the-art RF free-electron lasers (FELs). While first gain at 27 nm in a plasma-based FEL was achieved recently [9], the quality of bunches from LPA needs further improvement to fully compete with conventional accelerators in FEL applications. To this end, measuring the beam dynamics during the acceleration process is a crucial step towards understanding and controlling the acceleration mechanism inside plasma which ultimately governs the beam properties. Currently, particle-in-cell (PIC) simulations are the primary tool to determine the electron-beam-parameter evolution as state-of-the-art diagnostic methods are limited to observing the final state [10]. Existing schemes to detect the evolution of electron parameters in a plasma wakefield therefore require a modification of the final beam by changing the acceleration length [11–14]. Alternative noninvasive methods capable of determining electron parameters during evolution in plasma, such as streaked betatron radiation, are highly desirable and have been proposed [15]. However, they have yet to be experimentally demonstrated.

In this Letter, we report on the application of Thomson scattering [16] as a non-invasive technique for determining the energy evolution of an electron bunch during its acceleration inside a plasma wakefield. The measurements show excellent agreement with PIC simulations and had no discernible effect on the final state of the electron beam. This method enables in-situ characterization of the development of electron-bunch parameters with arbitrary wake drivers and injection mechanisms.

Thomson scattering is the elastic scattering of a photon and an electron, whereby the photon gains energy from a relativistic electron resulting in an x- or γ-ray in the direction of the electron. The energy $\hbar\omega_X$ of this photon for a scattering angle θ between electron and incoming photon is known as the cut-off energy and given by

$$\hbar\omega_X = 2\hbar\omega_0(1-\cos\theta)\gamma^2, \tag{1}$$

where γ is the Lorentz factor of the electron and $\hbar\omega_0$ is the initial photon energy. For the scattering of laser pulses and electron bunches, the Thomson spectrum is broadened [17–20] and its peak shifted to lower energies compared to the cut-off energy. The divergence of the electron bunch and the normalized vector potential a_0 of the scattering laser in particular can have a large influence on the resulting x-ray spectrum as described by Krämer *et al.* [19], who investigated this effect experimentally. To account for broadening effects, we introduce a factor Λ which describes the ratio of the peak of the produced x-ray spectrum and the cut-off energy, as the peak of the resulting x-ray spectrum has a lower dependence on broadening effects than e.g. the mean energy. By including this factor, the Lorentz factor of the electrons can thus be determined by measuring the spectrum of the scattered x-ray beam and rearranging Eq. 1 to

$$\gamma = \sqrt{\frac{\hbar\omega_X}{2\Lambda\hbar\omega_0\ (1-\cos\theta)}}. \tag{2}$$

The scattered radiation is typically in the hard x-ray range for highly relativistic electron bunches generated via LPA [21–27], such that the Thomson beam containing information about the electron bunch can be transported through the wakefield without significant plasma interaction. By overlapping the electron bunch and the Thomson laser at different locations inside plasma it is

* simon.bohlen@desy.de

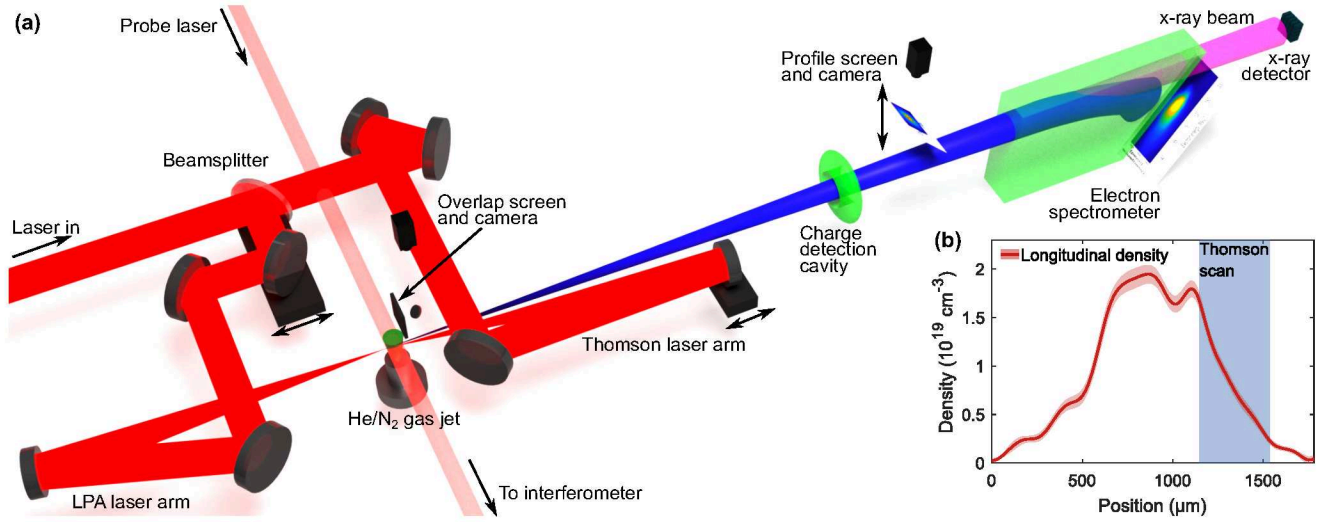

FIG. 1. a) Schematic of the experimental setup. b) Mean measured longitudinal plasma density profile with its standard deviation and the region where the Thomson measurement was performed.

therefore possible to gain information about the electron beam during its acceleration.

The experimental setup is schematically depicted in Fig. 1a. The laser was operated at a repetition rate of 1.4 Hz and its energy of 190 mJ was split using a 5 mm thick MgF beamsplitter, resulting in an energy of 125 mJ in the LPA laser arm and 65 mJ in the Thomson path. The LPA laser arm was focussed with an f/12 off-axis parabola to a $1/e^2$ intensity radius of (8.0 ± 0.2) µm. The FWHM pulse duration of the LPA laser was minimised to (26.9 ± 0.2) fs and measured with self-referenced spectral interferometry [28], resulting in a peak vacuum a_0 of 1.18. However, for optimisation of the generated electron bunches, the pulse was stretched using an acousto-optic dispersive filter [29]. The target was a 1 mm diameter gas jet operated with a gas mix of 99.5% helium and 0.5% nitrogen by weight and a backing pressure of (4.7 ± 0.1) bar. Interferometry measurements of the gas jet using a perpendicular probe beam revealed a peak plasma density of $(1.9 \pm 0.1) \times 10^{19}$ cm^{-3} as shown in the density profile in Fig. 1b. The Thomson laser arm was focused using a spherical mirror at an incidence angle of 4 degrees resulting in a FWHM spot size of 52 µm by 23 µm. The pulse length after the beamsplitter was measured to be (31.1 ± 0.6) fs, leading to a peak vacuum a_0 of 0.31 for the Thomson focus. The Thomson laser crossed the electron axis with an offset angle of 8 degrees to prevent backpropagation and damage of upstream laser optics and allow the x-ray beam to pass.

In order to change the longitudinal focus position of the Thomson laser the spherical mirror was mounted on a linear stage with its axis of movement parallel to the electron beam axis. To resynchronize the electron bunch and the Thomson laser correspondingly, a delay stage was placed inside the LPA laser arm. The two laser beams were overlapped in space using a screen which could be driven to a desired overlap plane. The focal plane of the Thomson laser was adjusted to the overlap plane using the linear stage of the spherical mirror. For the temporal alignment of the two laser beams the two generated ionisation channels in the gas plume were imaged using interferometry with an independently timed probe beam, similarly to Ref. [26].

Electron and x-ray beam diagnostics were installed downstream of the LPA. The charge of the bunches was measured using a non-invasive cavity-based resonator (DaMon) [30, 31], placed at a distance of 1.1 m from the electron source. The beam profile and pointing stability were measured on a DRZ-type phosphor screen [32, 33] which was driven into the electron beam at a distance of 1.3 m from the gas jet. The electron spectrum was measured using a spectrometer consisting of a 50 cm long vertically-dispersive dipole magnet with a field of 0.14 T and a DRZ screen, allowing for the observation of energies between 35 MeV and 250 MeV. The x-ray spectrum was taken using a HEXITEC detector [34, 35] which consists of 80 × 80 CdTe pixels with a size of 250 × 250 µm^2 and a thickness of 1 mm. To enable single photon counting, the detector was placed at a distance of 7.8 m from the Thomson interaction point, resulting in a measurement of the on-axis x-ray spectrum with an opening angle of ±1.25 mrad limited by the chip size.

To account for x-ray absorption from 1.7 mm of aluminium in the photon path between Thomson interaction point and the detector chip, and to include detection cross sections of the x-ray detector, a full reconstruction of the detector and the x-ray transport was performed in Geant4 [36–38]. In these simulations, x-ray beams with a mean energy between 30 keV and 100 keV and a spectral bandwidth similar to the measured spectra were simulated in steps of 1 keV. The resulting simulated HEXITEC spectra were then fitted to a sum of two Gaussian distributions with a separation of 25 keV to account for the escape peak shoulder [39] originating from

CdTe fluorescence x-rays (23 keV - 27 keV) leaving the detector [34, 35]. The spectral region around the fluorescence peak and events with an energy of less than 10 keV, which predominantly originate from detector noise, were excluded from the fit. An example of a Gaussian input spectrum, the energy deposited in the detector according to the Geant4 simulation, and the fit are depicted in Fig. 2a. The peaks of the fits of the deposited energy according to simulation for x-ray beams with initial peak energies between 30 keV and 100 keV are shown in Fig. 2b. The simulations show that the distribution of the deposited energy of the x-ray beams with a peak energy of less than 55 keV overestimates the mean energy of the incoming x-ray beams due to filtering of low-energy x-rays in the aluminium. The energy of x-ray beams with a peak energy above 65 keV is underestimated due to the lower quantum efficiency of the 1 mm thick CdTe for high-energy x-rays. To compensate for these effects, the peaks of measured Thomson spectra are corrected by the fit shown in Fig. 2b.

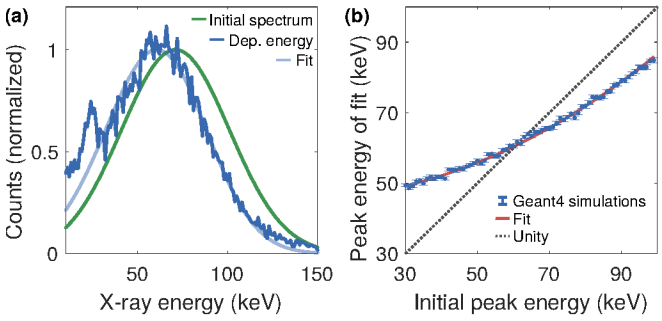

FIG. 2. (a) Simulation of an x-ray measurement with the HEXITEC. Shown are the initial spectrum of the x-ray beam (green line), the deposited energy of the x-ray beam (blue line) and the double Gaussian fit used to determine the peak of the deposited energy distribution (light blue line). (b) Peak of the deposited energy in the x-ray detector and 68% confidence intervals from fitting routine as a function of the initial peak input energy (blue dots). The red fit represents a look-up function used for a correction of the measured data. The grey dotted line indicates a slope where the input and output peaks are identical.

The electron beam was generated via self-truncated ionisation injection using a weakly relativistic laser [40, 41]. This resulted in spectrally stable and reproducible electron beams, as demonstrated in previous experiments using this injection method [42–44]. During the experiment, a FWHM pointing stability of the electron beams of 1.4 mrad was measured in the non-dispersive axis of the electron spectrometer. It was observed to be equal in both axes in dedicated pointing runs using the profile screen prior to the main experiments. The profile screen also yielded a beam divergence of (3.9 ± 0.7) mrad in the horizontal and (7.4 ± 1.6) mrad in the vertical plane. Owing to the specific experimental geometry and to ensure the x-ray detector occupancy was low enough to enable single photon counting while also minimizing the background of bremsstrahlung, the charge of the electron beams was kept low by reducing the laser energy to the stated values, limiting the charge to (2.7 ± 1.2) pC during this experiment. The electron beam energy was stable over the scan of more than 7000 shots to within 1 % with a spectral peak of the final electron energy of (61.3 ± 0.5) MeV. The normalised, average spectra of two consecutive sets of 340 shots each with and without the Thomson laser present is depicted in Fig. 3 highlighting the excellent spectral stability as well as the non-invasive character of the Thomson interaction.

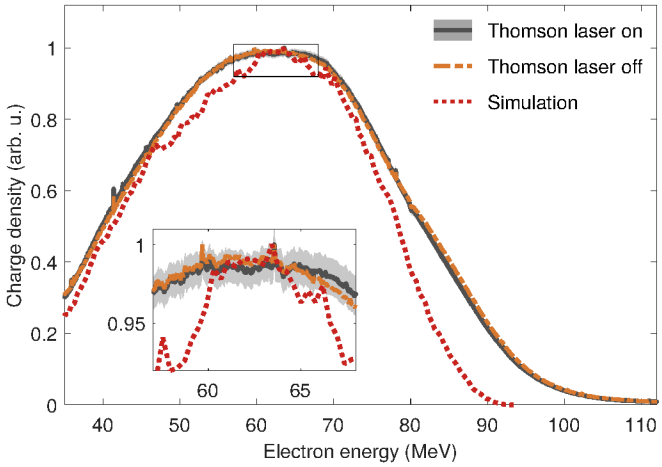

FIG. 3. Normalized electron spectrum of 340 shots at an overlap position inside the plasma with Thomson laser turned on (grey line) and the standard error from individual normalized shots (grey area) and the normalized electron spectrum at the same overlap position without the Thomson laser (orange dashed line). The error band of the run without Thomson laser is similar to the error band with Thomson laser. The spectrum obtained from PIC simulations is depicted as red dotted line. All lines are normalized individually. To highlight the agreement between the two measurements, the region around the peak is shown in more detail in the inset.

Using Thomson scattering, the electron beam energy was then measured at a total of 20 different interaction points of electron beam and Thomson laser, enabling a reconstruction of the electron beam energy evolution over a distance of 400 µm in the downramp of the plasma density profile, as shown in Fig. 4. At each overlap position, the signal of 280 shots was integrated on the x-ray detector. The bremsstrahlung background was determined in three dedicated background measurements for which the Thomson laser was blocked. The background-subtracted spectra were then fitted to the sum of two Gaussians as described earlier and shown in Fig. 2a. Afterwards, the peak of the fit was shifted according to the fit depicted in Fig. 2b to obtain the peak energy of the produced x-ray spectrum corrected for the absorption properties of materials in the beam path and quantum efficiency. The peak energy of the Thomson spectrum was then used to calculate the peak electron bunch energy using Eq. 2. The Λ factor was determined experimentally by compar-

ing the mean energy of the spectrometer measurement to the Thomson measurement at the last two interaction points, where the measurement suggests constant electron energies and the measured acceleration gradient is negligible. The found value of Λ of 0.92 agrees well with values shown by Krämer *et al.* in the range of 0.90 to 0.95 for using similar electron bunch and laser parameters [19]. In the measurement region, peak electron energies of (34 ± 5) MeV up to (61 ± 1) MeV were detected, showing the acceleration gradient to decrease in the downramp of the plasma from (265 ± 119) GV/m to (9 ± 4) GV/m. The measurement of the electron energy via Thomson scattering at overlap positions further inside the plasma was not possible, as the energy of the produced x-ray beam was below the detection threshold of 30 keV owing to absorption in the 1.7 mm aluminium shield in front of the detector. In Fig. 4a, the evolution of the electron beam energy is compared to the final electron energy measured using the electron spectrometer. As the absolute position of the overlap with respect to the density has an uncertainty of a few hundred µm, the experimental data set was shifted in the propagation axis to align with the simulation results by minimizing the least squares of the difference of measured data points and the simulated energy evolution (see below). The relative distance between the overlap positions was not affected by this shift and is well defined; the total uncertainty of the scan distance is less than 0.5%. The constant value of the final electron energy simultaneously measured using the spectrometer highlights the non-invasive nature of the demonstrated technique.

Simulations were performed using FBPIC [45, 46] to understand the energy gain in the plasma in more detail. In the simulation, laser and plasma parameters similar to those in the experiments were used. The plasma density profile depicted in Fig. 1b was imported, for the laser, a pulse duration of 35 fs, a $1/e^2$ intensity radius of 8.0 µm and a vacuum a_0 of 1.15 were chosen under the assumption of a Gaussian pulse in time and space. The simulation box with a length of 40 µm and a radius of 30 µm was divided in 2000 longitudinal and 128 radial grid points and 36 particles per cell. The laser focus position was scanned in the simulations to match the electron energies of the experiment and a vacuum focus at 1025 µm resulted in good agreement of the electron energy in the simulation and the spectrometer measurements as is shown in Fig. 3. The electron charge in the simulation was 1.8 pC, well within the standard error in the experiment. The comparison of the electron-beam-energy evolution and the resulting acceleration gradients of the in-situ Thomson measurements and the PIC simulation agree well as depicted in Fig. 4, substantiating the capability of the technique to accurately determine these parameters.

Thomson measurements could therefore be used to experimentally study the evolution of the electron bunch directly without dependence on a physics model or the complete and accurate determination of the experimental

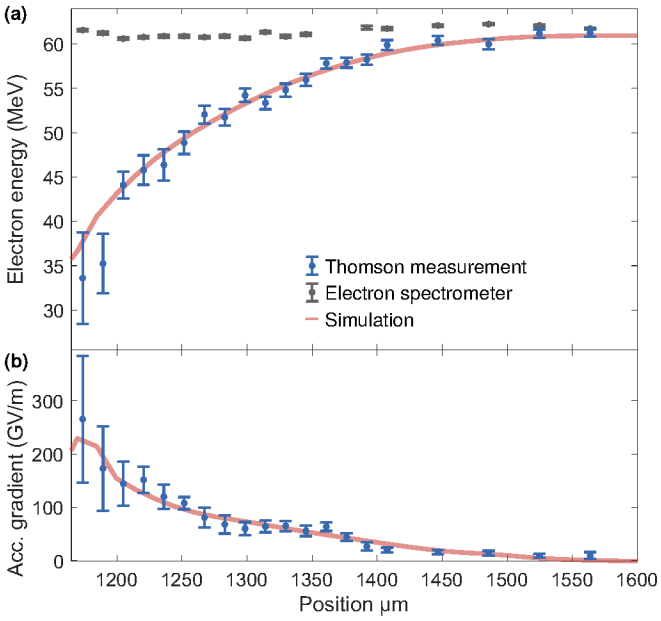

FIG. 4. a) Electron beam energy measured via Thomson scattering as function of the Thomson overlap position (blue). The final electron beam energy at each interaction point is shown as the average peak of Gaussian fits to the single electron spectra with its standard error (grey). The energy evolution obtained from the PIC simulation is shown as a red line, for better comparison again using Gaussian fits. b). Acceleration gradient as function of the overlap position. The acceleration gradient was calculated using a linear fit of ±3 data points. At the edges only available data points were included. The error bar displays the 68% confidence interval of the fit.

conditions. In combination with control of the longitudinal density, this diagnostic could therefore enable to improve schemes proposed to overcome the dephasing limit in LPA [47–49]. As it is sufficient to only detect the peak of the x-ray spectrum as demonstrated here, the measurement technique is compatible with the use of a single-shot x-ray spectrometer, available for a broad range of x- and γ-ray energies [50–52]. To improve the signal ratio, this method could also be used with traveling-wave Thomson scattering [53] while maintaining the non-invasive character of the measurement that requires the use of moderate intensities of the scattering laser [54]. In such a configuration, Thomson scattering could be used for a characterisation of the spectrum throughout the acceleration to optimise beam-loading of the beam required for low energy-spread electron bunches [55–57]. Furthermore, the technique may be extended to other electron parameters already measured using Thomson scattering such as emittance [27] or angular shape [19, 58, 59] in order to provide a complete picture of the electron bunch during its acceleration in the wakefield and consequently provide the necessary input to optimize the quality of LPA electron beams.

In summary, we demonstrate a non-invasive measure-

ment of the electron-bunch-energy evolution during its acceleration inside a plasma wakefield via Thomson scattering. Individual beam energy measurements over a 400 µm section of the plasma show an increase of the electron beam energy from (34 ± 5) MeV up to the final energy of (61 ± 1) MeV while the local acceleration gradient decreases from (265 ± 119) GV/m to (9 ± 4) GV/m. These results agree well with simulations, showing the capability to accurately measure the local energy and accelerating field experienced by the electron beam. Such non-invasive measurements will be crucial to understand the origin of beam-parameter changes, including emittance growth and energy spread in plasma accelerators and subsequently may play a key role in improving the quality of electron bunches e.g. for future FEL applications.

ACKNOWLEDGMENTS

The authors would like to thank M. Dinter, S. Karstensen, S. Kottler, K. Ludwig, F. Marutzky, A. Rahali, V. Rybnikov, and A. Schleiermacher for their engineering and technical support and the Central Laser Facility from the Science and Technology Facilities Council, UK for providing a HEXITEC detector. This work was supported by the Maxwell computational resources at DESY.

[1] T. Tajima and J. M. Dawson, Laser Electron Accelerator, Phys. Rev. Lett. **43**, 267 (1979).

[2] S. P. D. Mangles, C. D. Murphy, Z. Najmudin, A. G. R. Thomas, J. L. Collier, A. E. Dangor, E. J. Divall, P. S. Foster, J. G. Gallacher, C. J. Hooker, *et al.*, Monoenergetic beams of relativistic electrons from intense laserâ"plasma interactions, Nature **431**, 535 (2004).

[3] C. G. R. Geddes, C. Toth, J. van Tilborg, E. Esarey, C. B. Schroeder, D. Bruhwiler, C. Nieter, J. Cary, and W. P. Leemans, High-quality electron beams from a laser wakefield accelerator using plasma-channel guiding, Nature **431**, 538 (2004).

[4] J. Faure, Y. Glinec, A. Pukhov, S. Kiselev, S. Gordienko, E. Lefebvre, J.-P. Rousseau, F. Burgy, and V. Malka, A laserâ"plasma accelerator producing monoenergetic electron beams, Nature **431**, 541 (2004).

[5] H. T. Kim, K. H. Pae, H. J. Cha, I. J. Kim, T. J. Yu, J. H. Sung, S. K. Lee, T. M. Jeong, and J. Lee, Enhancement of electron energy to the multi-gev regime by a dual-stage laser-wakefield accelerator pumped by petawatt laser pulses, Phys. Rev. Lett. **111**, 165002 (2013).

[6] X. Wang, R. Zgadzaj, N. Fazel, Z. Li, S. A. Yi, X. Zhang, W. Henderson, Y. Y. Chang, R. Korzekwa, H. E. Tsai, *et al.*, Quasi-monoenergetic laser-plasma acceleration of electrons to 2 GeV, Nat. Commun. **4**, 1 (2013).

[7] W. P. Leemans, A. J. Gonsalves, H.-S. Mao, K. Nakamura, C. Benedetti, C. B. Schroeder, C. Tóth, J. Daniels, D. E. Mittelberger, S. S. Bulanov, *et al.*, Multi-GeV Electron Beams from Capillary-Discharge-Guided Subpetawatt Laser Pulses in the Self-Trapping Regime, Phys. Rev. Lett. **113**, 245002 (2014).

[8] A. J. Gonsalves, K. Nakamura, J. Daniels, C. Benedetti, C. Pieronek, T. C. H. de Raadt, S. Steinke, J. H. Bin, S. S. Bulanov, J. van Tilborg, *et al.*, Petawatt Laser Guiding and Electron Beam Acceleration to 8 GeV in a Laser-Heated Capillary Discharge Waveguide, Phys. Rev. Lett. **122**, 084801 (2019).

[9] W. Wang, K. Feng, L. Ke, C. Yu, Y. Xu, R. Qi, Y. Chen, Z. Qin, Z. Zhang, M. Fang, *et al.*, Free-electron lasing at 27 nanometres based on a laser wakefield accelerator, Nat. 2021 5957868 **595**, 516 (2021).

[10] M. C. Downer, R. Zgadzaj, A. Debus, U. Schramm, and M. C. Kaluza, Diagnostics for plasma-based electron accelerators, Rev. Mod. Phys. **90**, 035002 (2018).

[11] J. Faure, C. Rechatin, A. Norlin, A. Lifschitz, Y. Glinec, and V. Malka, Controlled injection and acceleration of electrons in plasma wakefields by colliding laser pulses, Nature **444**, 737 (2006).

[12] K. K. Swanson, H. E. Tsai, S. K. Barber, R. Lehe, H. S. Mao, S. Steinke, J. Van Tilborg, K. Nakamura, C. G. Geddes, C. B. Schroeder, *et al.*, Control of tunable, monoenergetic laser-plasma-accelerated electron beams using a shock-induced density downramp injector, Phys. Rev. Accel. Beams **20**, 10.1103/PhysRevAccelBeams.20.051301 (2017).

[13] D. E. Cardenas, S. Chou, E. Wallin, J. Xu, L. Hofmann, A. Buck, K. Schmid, D. E. Rivas, B. Shen, A. Gonoskov, *et al.*, Electron bunch evolution in laser-wakefield acceleration, Phys. Rev. Accel. Beams **23**, 112803 (2020).

[14] K. Poder, J. C. Wood, N. C. Lopes, J. M. Cole, S. Alatabi, P. S. Foster, C. Kamperidis, O. Kononenko, C. A. J. Palmer, D. Rusby, *et al.*, Multi-GeV electron acceleration in wakefields strongly driven by oversized laser spots, submitted (2020).

[15] Y. Ma, D. Seipt, S. J. D. Dann, M. J. V. Streeter, C. A. J. Palmer, L. Willingale, and A. G. R. Thomas, Angular streaking of betatron X-rays in a transverse density gradient laser-wakefield accelerator, Phys. Plasmas **25**, 113105 (2018).

[16] J. J. Thomson, Conductivity of Electricity through Gases, (Cambridge Univ. Press. (1906).

[17] W. J. Brown, S. G. Anderson, C. P. J. Barty, S. M. Betts, R. Booth, J. K. Crane, R. R. Cross, D. N. Fittinghoff, D. J. Gibson, F. V. Hartemann, *et al.*, Experimental characterization of an ultrafast Thomson scattering x-ray source with three-dimensional time and frequency-domain analysis, Phys. Rev. Spec. Top. - Accel. Beams **7**, 23 (2004).

[18] S. G. Rykovanov, C. G. R. Geddes, J.-L. Vay, C. B. Schroeder, E. Esarey, and W. P. Leemans, Quasi-monoenergetic femtosecond photon sources from Thomson Scattering using laser plasma accelerators and plasma channels, J. Phys. B At. Mol. Opt. Phys. **47**, 234013 (2014).

[19] J. M. Krämer, A. Jochmann, M. Budde, M. Bussmann, J. P. Couperus, T. E. Cowan, A. Debus, A. Köhler, M. Kuntzsch, A. Laso García, *et al.*, Making spectral shape measurements in inverse Compton scattering a tool

for advanced diagnostic applications, Sci. Rep. **8**, 1398 (2018).

[20] T. Brümmer, A. Debus, R. Pausch, J. Osterhoff, and F. Grüner, Design study for a compact laser-driven source for medical X-ray fluorescence imaging, Phys. Rev. Accel. Beams **23**, 031601 (2020).

[21] H. Schwoerer, B. Liesfeld, H. P. Schlenvoigt, K. U. Amthor, and R. Sauerbrey, Thomson-backscattered X rays from laser-accelerated electrons, Phys. Rev. Lett. **96**, 10.1103/PhysRevLett.96.014802 (2006).

[22] K. Ta Phuoc, S. Corde, C. Thaury, V. Malka, A. Tafzi, J. P. Goddet, R. C. Shah, S. Sebban, and A. Rousse, All-optical Compton gamma-ray source, Nat. Photonics **6**, 308 (2012), arXiv:1301.3973.

[23] S. Chen, N. D. Powers, I. Ghebregziabher, C. M. Maharjan, C. Liu, G. Golovin, S. Banerjee, J. Zhang, N. Cunningham, A. Moorti, *et al.*, MeV-energy X rays from inverse compton scattering with laser-wakefield accelerated electrons, Phys. Rev. Lett. **110**, 155003 (2013).

[24] N. D. Powers, I. Ghebregziabher, G. Golovin, C. Liu, S. Chen, S. Banerjee, J. Zhang, and D. P. Umstadter, Quasi-monoenergetic and tunable X-rays from a laser-driven Compton light source, Nat. Photonics **8**, 28 (2014).

[25] G. Sarri, D. J. Corvan, W. Schumaker, J. M. Cole, A. Di Piazza, H. Ahmed, C. Harvey, C. H. Keitel, K. Krushelnick, S. P. Mangles, *et al.*, Ultrahigh brilliance multi-MeV γ-ray beams from nonlinear relativistic thomson scattering, Phys. Rev. Lett. **113**, 224801 (2014).

[26] K. Khrennikov, J. Wenz, A. Buck, J. Xu, M. Heigoldt, L. Veisz, and S. Karsch, Tunable All-Optical Quasimonochromatic Thomson X-Ray Source in the Nonlinear Regime, Phys. Rev. Lett. **114**, 195003 (2015).

[27] G. Golovin, S. Banerjee, C. Liu, S. Chen, J. Zhang, B. Zhao, P. Zhang, M. Veale, M. Wilson, P. Seller, *et al.*, Intrinsic beam emittance of laser-accelerated electrons measured by x-ray spectroscopic imaging, Sci. Rep. **6**, 24622 (2016).

[28] T. Oksenhendler, S. Coudreau, N. Forget, V. Crozatier, S. Grabielle, R. Herzog, O. Gobert, and D. Kaplan, Self-referenced spectral interferometry, Appl. Phys. B Lasers Opt. **99**, 7 (2010).

[29] P. Tournois, Acousto-optic programmable dispersive filter for adaptive compensation of group delay time dispersion in laser systems, Opt. Commun. **140**, 245 (1997).

[30] D. Lipka, W. Kleen, J. Lund-Nielsen, D. Nölle, S. Vilcins, and V. Vogel, Dark current monitor for the European XFEL, in *Proc. DIPAC2011* (JACow, Hamburg, Germany, 2011) pp. 572–574.

[31] D. Lipka, J. Lund-Nielsen, and M. Seebach, Resonator for charge measurement at REGEA, in *Proc. IBIC2013* (JACow, Oxford, UK, 2013) pp. 872 – 875.

[32] T. Kurz, J. P. Couperus, J. M. Krämer, H. Ding, S. Kuschel, A. Köhler, O. Zarini, D. Hollatz, D. Schinkel, R. D'Arcy, *et al.*, Calibration and cross-laboratory implementation of scintillating screens for electron bunch charge determination, Rev. Sci. Instrum. **89**, 093303 (2018).

[33] J.-P. Schwinkendorf, S. Bohlen, J. Couperus CabadaÄŸ, H. Ding, A. Irman, S. Karsch, A. Köhler, J. Krämer, T. Kurz, S. Kuschel, *et al.*, Charge calibration of DRZ scintillation phosphor screens, J. Instrum. **14** (09), P09025.

[34] P. Seller, S. Bell, R. J. Cernik, C. Christodoulou, C. K. Egan, J. A. Gaskin, S. Jacques, S. Pani, B. D. Ramsey, C. Reid, *et al.*, Pixellated Cd(Zn)Te high-energy X-ray instrument., J. Instrum. **6** (12).

[35] M. C. Veale, P. Seller, M. Wilson, and E. Liotti, HEXITEC: A High-Energy X-ray Spectroscopic Imaging Detector for Synchrotron Applications, Synchrotron Radiat. News **31**, 28 (2018).

[36] S. Agostinelli, J. Allison, K. Amako, J. Apostolakis, H. Araujo, P. Arce, M. Asai, D. Axen, S. Banerjee, G. Barrand, *et al.*, Geant4â"a simulation toolkit, Nucl. Instruments Methods Phys. Res. Sect. A Accel. Spectrometers, Detect. Assoc. Equip. **506**, 250 (2003).

[37] J. Allison, K. Amako, J. Apostolakis, H. Araujo, P. Arce Dubois, M. Asai, G. Barrand, R. Capra, S. Chauvie, R. Chytracek, *et al.*, Geant4 developments and applications, IEEE Trans. Nucl. Sci. **53**, 270 (2006).

[38] J. Allison, K. Amako, J. Apostolakis, P. Arce, M. Asai, T. Aso, E. Bagli, A. Bagulya, S. Banerjee, G. Barrand, *et al.*, Recent developments in Geant4, Nucl. Instruments Methods Phys. Res. Sect. A Accel. Spectrometers, Detect. Assoc. Equip. **835**, 186 (2016).

[39] R. H. Redus, J. A. Pantazis, T. J. Pantazis, A. C. Huber, and B. J. Cross, Characterization of CdTe detectors for quantitative X-ray spectroscopy, in *IEEE Trans. Nucl. Sci.*, Vol. 56 (2009) pp. 2524–2532.

[40] M. Zeng, M. Chen, Z.-M. Sheng, W. B. Mori, and J. Zhang, Self-truncated ionization injection and consequent monoenergetic electron bunches in laser wakefield acceleration, Phys. Plasmas **21**, 030701 (2014).

[41] C. Kamperidis, V. Dimitriou, S. P. Mangles, A. E. Dangor, and Z. Najmudin, Low energy spread electron beams from ionization injection in a weakly relativistic laser wakefield accelerator, Plasma Phys. Control. Fusion **56**, 084007 (2014).

[42] M. Mirzaie, S. Li, M. Zeng, N. A. M. Hafz, M. Chen, G. Y. Li, Q. J. Zhu, H. Liao, T. Sokollik, F. Liu, *et al.*, Demonstration of self-truncated ionization injection for GeV electron beams, Sci. Rep. **5**, 14659 (2015).

[43] J. P. Couperus, R. Pausch, A. Köhler, O. Zarini, J. M. Krämer, M. Garten, A. Huebl, R. Gebhardt, U. Helbig, S. Bock, *et al.*, Demonstration of a beam loaded nanocoulomb-class laser wakefield accelerator, Nat. Commun. **8**, 487 (2017).

[44] A. Irman, J. P. Couperus, A. Debus, A. Köhler, J. M. Krämer, R. Pausch, O. Zarini, and U. Schramm, Improved performance of laser wakefield acceleration by tailored self-truncated ionization injection, Plasma Phys. Control. Fusion **60**, 044015 (2018).

[45] R. Lehe, M. Kirchen, I. A. Andriyash, B. B. Godfrey, and J. L. Vay, A spectral, quasi-cylindrical and dispersion-free Particle-In-Cell algorithm, Comput. Phys. Commun. **203**, 66 (2016), arXiv:1507.04790.

[46] S. Jalas, I. Dornmair, R. Lehe, H. Vincenti, J. L. Vay, M. Kirchen, and A. R. Maier, Accurate modeling of plasma acceleration with arbitrary order pseudo-spectral particle-in-cell methods, Phys. Plasmas **24**, 033115 (2017), arXiv:1611.05712.

[47] P. Sprangle, B. Hafizi, J. R. Peñano, R. F. Hubbard, A. Ting, C. I. Moore, D. F. Gordon, A. Zigler, D. Kaganovich, and T. M. o. Antonsen, Wakefield generation and GeV acceleration in tapered plasma channels, Phys. Rev. E - Stat. Nonlinear, Soft Matter Phys. **63**, 564051 (2001).

[48] E. Guillaume, A. Döpp, C. Thaury, K. Ta Phuoc, A. Lifschitz, G. Grittani, J. P. Goddet, A. Tafzi, S. W. Chou, L. Veisz, *et al.*, Electron Rephasing in a Laser-Wakefield Accelerator, Phys. Rev. Lett. **115**, 155002 (2015).

[49] J. D. Sadler, C. Arran, H. Li, and K. A. Flippo, Overcoming the dephasing limit in multiple-pulse laser wakefield acceleration, Phys. Rev. Accel. Beams 10.1103/physrevaccelbeams.23.021303 (2020), arXiv:2001.09108.

[50] D. J. Corvan, G. Sarri, and M. Zepf, Design of a compact spectrometer for high-flux MeV gamma-ray beams, Rev. Sci. Instrum. **85**, 065119 (2014).

[51] K. T. Behm, J. M. Cole, A. S. Joglekar, E. Gerstmayr, J. C. Wood, C. D. Baird, T. G. Blackburn, M. Duff, C. Harvey, A. Ilderton, *et al.*, A spectrometer for ultrashort gamma-ray pulses with photon energies greater than 10 MeV, Rev. Sci. Instrum. **89**, 113303 (2018).

[52] A. Hannasch, A. L. Garcia, M. LaBerge, R. Zgadzaj, A. Köhler, J. P. C. CabadaÄŸ, O. Zarini, T. Kurz, A. Ferrari, M. Molodtsova, *et al.*, Compact spectroscopy of keV to MeV X-rays from a laser wakefield accelerator, Sci. Reports 2021 111 **11**, 1 (2021).

[53] Q. Chen, V. Horný, R. Syed, and D. Umstadter, Traveling-wave Thomson scattering for electron-beam spectroscopy, Phys. Rev. Accel. Beams **24**, 032901 (2021).

[54] M. Streeter and Z. Najmudin, Compton recoil effects in staging of laser wakefield accelerators, Phys. Rev. Accel. Beams **23**, 071602 (2020).

[55] M. Tzoufras, W. Lu, F. S. Tsung, C. Huang, W. B. Mori, T. Katsouleas, J. Vieira, R. A. Fonseca, and L. O. Silva, Beam Loading in the Nonlinear Regime of Plasma-Based Acceleration, Phys. Rev. Lett. **101**, 145002 (2008).

[56] C. A. Lindstrøm, J. M. Garland, S. Schröder, L. Boulton, G. Boyle, J. Chappell, R. D'Arcy, P. Gonzalez, A. Knetsch, V. Libov, *et al.*, Energy-Spread Preservation and High Efficiency in a Plasma-Wakefield Accelerator, Phys. Rev. Lett. **126**, 014801 (2021).

[57] M. Kirchen, S. Jalas, P. Messner, P. Winkler, T. Eichner, L. Hübner, T. Hülsenbusch, L. Jeppe, T. Parikh, M. Schnepp, *et al.*, Optimal Beam Loading in a Laser-Plasma Accelerator, Phys. Rev. Lett. **126**, 174801 (2021).

[58] K. Chouffani, F. Harmon, D. Wells, J. Jones, and G. Lancaster, Determination of electron beam parameters by means of laser-Compton scattering, Phys. Rev. Spec. Top. - Accel. Beams **9**, 050701 (2006).

[59] A. Jochmann, A. Irman, M. Bussmann, J. P. Couperus, T. E. Cowan, A. D. Debus, M. Kuntzsch, K. W. D. Ledingham, U. Lehnert, R. Sauerbrey, *et al.*, High Resolution Energy-Angle Correlation Measurement of Hard X Rays from Laser-Thomson Backscattering, Phys. Rev. Lett. **111**, 114803 (2013).